δ-biased Josephson tunnel junctions

R. Monaco*
Istituto di Cibernetica del CNR, 80078 Pozzuoli, Italy
and Dipartimento di Fisica, Università di Salerno, 84081 Baronissi, Italy

J. Mygind
DTU Physics, Technical University of Denmark, B309, DK-2800 Lyngby, Denmark

V. P. Koshelets and P. Dmitriev
Institute of Radio Engineering and Electronics, Russian Academy of Science, Mokhovaya 11, Bldg. 7, 125009 Moscow, Russia
(Received 8 December 2009; published 12 February 2010)

The behavior of a long Josephson tunnel junction drastically depends on the distribution of the dc bias current. We investigate the case in which the bias current is fed in the central point of a one-dimensional junction. Such junction configuration has been recently used to detect the persistent currents circulating in a superconducting loop. Analytical and numerical results indicate that the presence of fractional vortices leads to remarkable differences from the conventional case of uniformly distributed dc bias current. The theoretical findings are supported by detailed measurements on a number of δ-biased samples having different electrical and geometrical parameters.

DOI: 10.1103/PhysRevB.81.054506 PACS number(s): 03.70.+k, 05.70.Fh, 03.65.Yz

I. INTRODUCTION

Symmetry principles and how they are broken are fundamental concepts in physics. A recent experiment[1,2] demonstrated that the symmetry can spontaneously break during the fast superconducting phase transition of a metal ring and both fluxoids or antifluxoids can be trapped in the ring while its temperature crosses the superconducting critical temperature. This phenomenon was predicted a long time ago as one among several possible condensed-matter *cosmological* experiments[3] to check the validity of the *causality* principle in the early Universe.[4] In the experiment of Ref. 1 the presence of the persistent currents associated with the flux trapped in the ring relied on the radial magnetic field modulation of the critical current of a planar Josephson tunnel junction (JTJ) having the peculiar configuration shown in Fig. 1(a). It consists of a ring-shaped junction *cut* at some point with the bias current fed at the diametrically opposite point. The cut leaves a *gapped* annular junction and relieves the junction from the constraint of the 2π-periodic boundary condition of annular junctions.[5] In that experiment the ring itself acted as the junction base electrode while the top electrode had the shape of a circular arc of about 300°. Later on it will be demonstrated that a gapped annular junction in a radially uniform magnetic field H_r is topologically equivalent to a linear junction in an in-plane uniform field $H_\parallel$ as that depicted in Fig. 1(b).

The task of this work is to study the properties of a δ *-biased* or *single-point injected* overlap Josephson tunnel junction whose physical length is L, i.e., $-L/2 \leq X \leq L/2$ and whose width is W, i.e., $-W/2 \leq Y \leq W/2$. To simplify the analysis, we assume that Josephson current density J_c is uniform over the barrier area and that the junction width W is smaller than the Josephson penetration depth λ_J. Ideally, the bias current is fed to the junction by infinitely narrow electrodes. In real devices the δ-bias approximation is achieved as far as the electrodes carrying the bias current in and out of the tunnel barrier are much narrower than the junction Josephson penetration depth λ_j; however, for very long junctions, it is only required that they are narrower than the junction length L. In window-type JTJs one more requirement is that the passive region surrounding the tunnel area, the so-called *idle region*,[6–8] needs to be narrower than the current-carrying electrodes otherwise the bias current diffuses before entering the barrier and the sharp bias profile gets smeared. We will consider both intermediate length ($L \simeq \lambda_j$) and long ($L \gg \lambda_j$) JTJs (the behavior of small junctions is not affected by the bias profile). We remark that with the current injected at the junction extremities we recover the well-known case of so-called *in-line* configuration treated by pioneering works on long JTJs soon after the discovery of the Josephson effect.[9–11] For in-line JTJs it is important to distinguish between the symmetric[10,11] and asymmetric configuration:[9,10] the former is achieved when the bias current enters at one extremity and exits at the opposite one while the latter is obtained when the bias current enters and exits from the same extremity. Since in this paper we will only consider the case in which the bias current is fed in the middle of the

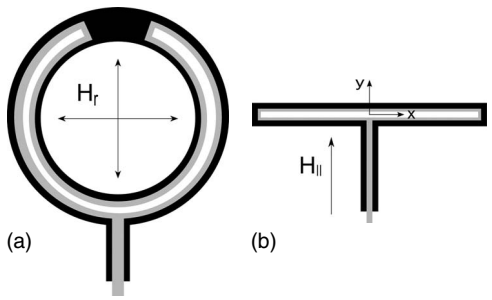

FIG. 1. (a) Gapped annular and (b) linear δ-biased Josephson tunnel junctions. The base electrodes are in black, the top electrodes are in gray, and the junction areas are white. A gapped annular junction in a radially uniform magnetic field H_r is topologically equivalent to a linear junction in an in- plane uniform field $H_\parallel$.

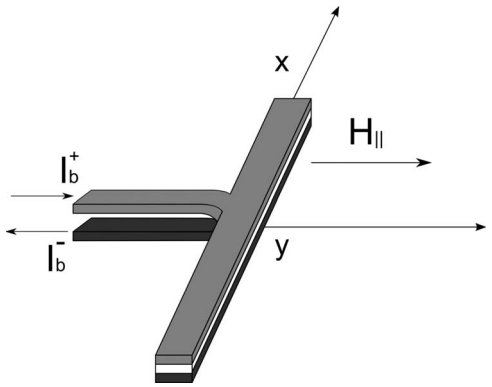

FIG. 2. Three-dimensional sketch of a centrally injected δ-biased linear planar Josephson tunnel junction.

junction long dimension, for symmetry reasons, we do not need to specify the electrode configuration. Nevertheless the more general situation in which the bias current enters and leaves in two generic lateral points along the junction will deserve consideration in the future. We will show that, with the bias current centrally injected, both the static and dynamic junction properties reveal interesting phenomena whose understanding will serve as a base for the study of more general cases. In this regard, a considerable attention has been recently given to the case of $0-\pi$ transition Josephson tunnel junction obtained by closely situated current injectors.[12,13] For the sake of completeness it is worth to remark that the lateral point injected bias was already treated in the literature but only in the limit of infinitely long JTJs.[14–16]

II. MODEL

It can be shown that for a δ-biased JTJ, as that sketched in Fig. 2, the gauge-invariant phase difference ϕ of the order parameters of the superconductors on each side of the tunnel barrier obeys the static or dc perturbed sine-Gordon equation,

$$\lambda_j^2 \frac{d^2\phi}{dX^2} = \sin\,\phi(X) - \gamma\delta\left(\frac{X}{\lambda_j}\right),$$

in which the term $\gamma = I_b/I_0$ is the external bias current I_b normalized to $I_0 = J_c LW$ and δ is the δ function. In normalized units of $x = X/\lambda_j$, the above partial differential equation (PDE) becomes

$$\frac{d^2\phi}{dx^2} = \sin\,\phi(x) - \gamma\delta(x). \tag{1}$$

If the time t replaces x in Eq. (1) and a new phase $\psi = \phi - \pi$ is defined, we obtain the equation for a lossless pendulum with an applied torque like a train of pulses with unitary period. In this framework, the boundary conditions will become constraints on the pendulum angular velocity half period before and after each pulse.

It is possible to derive that, introducing the Heaviside step function $\mathcal{H}(x)$, the Lagrangian density $\mathcal{L}$ of our system is constant along the barrier

$$\mathcal{L} = \frac{\phi_x^2}{2} + \cos\,\phi + \gamma\phi_x(0)\mathcal{H}(x).$$

By subtracting the constant quantity $\gamma\phi_x(0)/2$, we can rewrite the last expression as

$$\frac{\phi_x^2}{2} + \cos\,\phi + \frac{\gamma\phi_x(0)}{2}\mathrm{sgn}(x) = C, \tag{2}$$

with C being a constant depending on both the external bias and magnetic field. Note that if $\phi_x(x)$ is discontinuous in $x = 0$, then $2\phi_x(0) = \phi_x(0+) + \phi_x(0-)$. The first two terms in Eq. (2) are related to the system free-energy density $\mathcal{E}(x) = 1 - \cos\,\phi - \phi_x^2/2$ while the last term represents the two-level potential $\mathcal{U}(x)$ generated by the δ-shaped forcing term.

Boundary conditions

The magnetic Josephson equation[17] states that the phase gradient is proportional to the magnetic field

$$\nabla\phi = \frac{2\pi d_e \mu_0}{\Phi_0}\mathbf{H}\times\mathbf{n}, \tag{3}$$

where $\mathbf{n}$ is a unit vector normal to the insulating barrier separating the two superconducting electrodes. If the two superconducting films have thicknesses $d_{1,2}$ and London penetration depths $\lambda_{L1,2}$ and t_j is the barrier thickness, then the effective magnetic penetration d_e is given by,[18]

$$d_e = t_j + \lambda_{L1}\tanh\frac{d_1}{2\lambda_{L1}} + \lambda_{L2}\tanh\frac{d_2}{2\lambda_{L2}},$$

which, in the case of thick superconducting films ($d_i \gg \lambda_{Li}$), reduces to $d_e \approx \lambda_{L1} + \lambda_{L2}$ (since always $d_i \gg t_j$).

From Eq. (3) it follows that, for a linear JTJ in an external uniform field $H_\parallel$ applied in the junction plane perpendicular to its length L, the boundary conditions are

$$\left.\frac{d\phi}{dX}\right|_{X=\pm L/2} = \kappa H_\parallel, \tag{4}$$

with $\kappa = 2\pi d_e\mu_0/\Phi_0$. Being $\lambda_j^{-2} = 2\pi d_e\mu_0 J_c/\Phi_0 = \kappa J_c$ (Φ_0 is the magnetic-flux quantum and μ_0 is the vacuum permeability), we have $\kappa\lambda_j = 1/J_c\lambda_j$. Introducing the critical field H_c^* for a unitary junction with a Fraunhofer magnetic diffraction pattern $H_c^* = \Phi_0/(\mu_0 d_e \lambda_j) = 2\pi J_c\lambda_j = 2\pi/\kappa\lambda_j$, we get $\kappa\lambda_j = 2\pi/H_c^*$. In normalized units of $h = \kappa\lambda_j H_\parallel = 2\pi H_\parallel/H_c^* = H_\parallel/J_c\lambda_j$, the boundary conditions (4) for Eq. (1) are

$$\left.\frac{d\phi}{dx}\right|_{x=\pm l/2} = h, \tag{5}$$

in which we have introduced the junction normalized length $l = L/\lambda_j$. Note that, with this notations, the normalized critical field h_c^* of a short JTJ equals $2\pi/l$. For the gapped annular junction in a radially uniform field H_r, the boundary conditions for the PDE in Eq. (1) are independent on the gap angle[19] and coincide with those in Eq. (5), but now with $h = 2\pi H_r/H_c^*$. In other words, a linear junction in an in-plane field $H_\parallel$ and a gapped annular junction in a radial field H_r are governed by the same PDE with the same boundary condi-

tions. Therefore, for the remaining of the paper we will use the properly normalized field h both for linear and gapped annular JTJs. A radial magnetic field can be generated by a current flowing in a control line in the shape of a loop concentric to the annulus; however, the simplest way[1] is to have a ring-shaped base electrode and to apply an external field perpendicular to it to induce tangential screening currents proportional to the applied field. The only disadvantage of this method is that the effective radial field felt by the gapped annular junction depends on geometrical factors such as the ring inner and outer radii and the junction position relative to the ring. The radial dependence of the current circulating in a superconducting ring has been calculated under many different conditions,[20] and, among other things, it was found that the shielding currents mainly flow on the outer side of the ring.

From Eqs. (1) and (5), we have that the junction Josephson current i_j is proportional to the bias current; in fact, being $\int_{-a}^{a}\delta(x)dx=1$, we get

$$i_j \equiv \frac{I_j}{I_0} = \frac{1}{l}\int_{-l/2}^{l/2} \sin\,\phi(x)dx = \frac{1}{l}\left(\left.\frac{d\phi}{dx}\right|_{x=+l/2} - \left.\frac{d\phi}{dx}\right|_{x=-l/2}\right) + \frac{\gamma}{l} = \frac{\gamma}{l}, \tag{6}$$

that is, for a fixed bias current I_b, the zero-voltage current I_j passing through a δ-biased JTJ is inversely proportional to its normalized length ($I_j=I_b\lambda_j/L$). In the well-known case of an overlap JTJ with uniform bias $\gamma(x)=\gamma_u$, it would be $i_j=\gamma_u$ (i.e., $I_j=I_b$), meaning that γ_u cannot exceed unity. In contrast, Eq. (6) implies that for δ-biased junctions the largest value γ_c that the normalized bias current can achieve is determined by the junction normalized length. Later on it will be found that, in our case, $|\gamma|\leq 4$.

The jump in the phase gradient at the injection point (the axis origin in case) can be calculated directly from Eq. (1). For any $0<x_0<l/2$ we can write

$$\left.\frac{d\phi}{dx}\right|_{x=x_0} - \left.\frac{d\phi}{dx}\right|_{x=-x_0} = \int_{-x_0}^{x_0}[\sin\,\phi(x) - \gamma\delta(x)]dx = \int_{-x_0}^{x_0}\sin\,\phi(x)dx - \gamma.$$

Taking the limit $x_0\to 0$, the integral vanishes, being $\phi(x)$ a continuous function; then the phase derivative jumps at the injection point $x=0$,

$$\left.\frac{d\phi}{dx}\right|_{x=0+} - \left.\frac{d\phi}{dx}\right|_{x=0-} = -\gamma. \tag{7}$$

This equation was first reported by Kuprianov *et al.*[14] [see also Ref. 15 at (par.8.5)] for JTJs with lateral single-point injection. We can rewrite Eq. (7) as

$$\left.\frac{d\phi}{dx}\right|_{x=0-} = -\left.\frac{d\phi}{dx}\right|_{x=0+} = \gamma/2 + h_0, \tag{8}$$

in which the constant h_0 is a measure of the (exponential) penetration of the external magnetic field (if any) into the center of the junction; in general, h_0 cannot be determined *a priori*.

III. ANALYTICAL APPROXIMATE SOLUTIONS FOR LONG JTJs

In this section we will discuss the possible analytical approaches to determine the phase profile of a point-injected long JTJ in the Meissner state. In absence of an external bias γ and a magnetic field h the Josephson phase profile $\phi(x)$ is identically equal to zero. If γ and h are sufficiently small, then $|\phi(x)|\ll 1$, so that Eq. (1) can be linearized, being $\sin\,\phi\approx\phi$. Barone *et al.*[21,22] pointed out that a piecewise linear current phase relationship $j_j=\chi^2\phi\leq 1$ (with $\chi\in[0.5,1]$) can correctly handle the case when $|\phi(x)|<\pi/2$. Obviously in a linear approximation the phase profile looses its correct structure within the scale of λ_j but averaged results such as the Josephson current are not significantly affected by the approximation. However, as will be shown later on, for δ-biased JTJs in the Meissner state it is $|\phi(x)|\leq\pi$ so that the piecewise linear approximation fails and a cubic approximation, $\sin\,\phi\simeq\alpha\phi-\beta\phi^3$, can be conveniently adopted leading to a Duffing-type differential equation for the oscillation of a soft ($\alpha,\beta>0$) spring system. In the special case of the underdamped and unforced Duffing equation, exact solutions can be written in terms of Jacobi's elliptic functions.[23] Further, approximate solutions of the forced Duffing equation could be found using the perturbation methods[24] when $\beta\ll\alpha$. However, simple solutions, Eq. (1), can be readily obtained in the approximation of very long junctions.

A. $h\neq 0$ and $\gamma=0$, $l/2>2\pi$

We begin with the case of no externally applied magnetic field which, in the well-studied case of uniform bias, results in a constant phase profile $\phi(x)=\sin^{-1}\,\gamma_u\ (\mathrm{mod}\,2\pi)$. For symmetry reasons, in the case of δ-biased JTJs, the solution of Eq. (1) has to be an even function $\phi^e(x)$. Therefore its gradient is an odd function, $\phi_x^e(x)+\phi_x^e(-x)=0$, meaning that $h_0=0$ in Eq. (8). With $h_0=0$, Eq. (8) provides two extra conditions on the phase left and right derivative at the injection point.

$$\left.\frac{d\phi}{dx}\right|_{x=0-} = -\left.\frac{d\phi}{dx}\right|_{x=0+} = \gamma/2. \tag{9}$$

For $l\gg 4\pi$ (strictly in the limit $l\to\infty$), an approximate solution of Eq. (1) fulfilling the above conditions is a cusplike function,

$$\phi^e(x) = \pm 4\,\tan^{-1}\exp-(|x|+\xi), \tag{10}$$

in which ξ is a non-negative constant set by the bias current γ; Eq. (10) can also be cast in the form:[9] $\sin\,\phi^e(x)/2 = \pm\,\mathrm{sech}(|x|+\xi)$. It is $\phi^e(\pm\infty)=\phi_x^e(\pm\infty)=0$ and $\phi^e(0) = \pm 4\,\tan^{-1}\exp(-\xi)$. The sign in front of Eq. (10) concords with that of the external bias current. With $\xi=0$ (and positive γ), then $\phi^e(0)=\pi$, meaning that Eq. (10) corresponds to a semifluxon (π jump) on the left side of the junction and antisemifluxon ($-\pi$ jump) on the right side, as shown in Figs. 3(a)–3(d) for $-10<x<10$ (we observe that, as required,

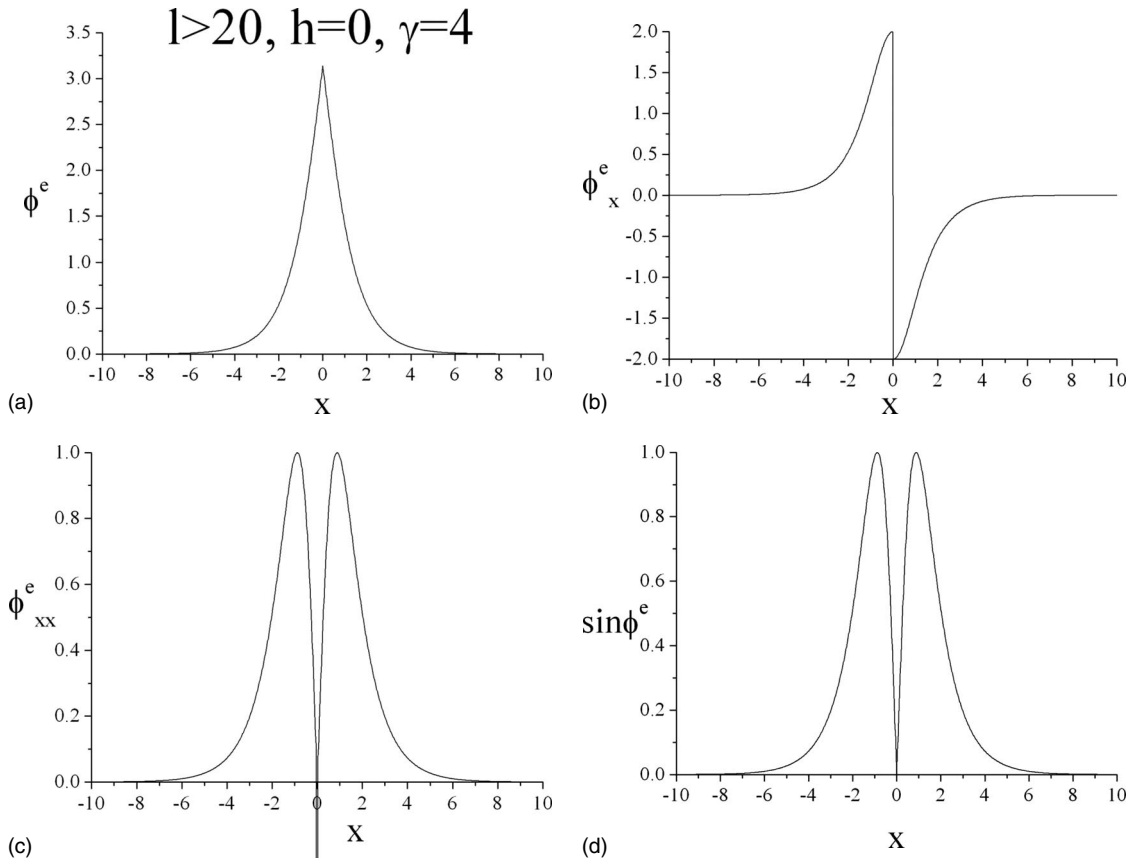

FIG. 3. (a) Phase profile $\phi^e(x)$ for an infinitely long δ-biased JTJ as in Eq. (10) with $\xi=0$ corresponding to $\gamma=4$, for $x\in[-10,10]$. (b), (c), and (d) show, respectively, $\phi^e_x(x)$, $\phi^e_{xx}(x)$, and $\sin\phi^e(x)$. It is $\cos\phi^e(x)=1-[\phi^e_x(x)]^2/2$.

$\phi_{xx}=\sin\phi$, everywhere, but for $x=0$). The dependence of ξ on γ can be found observing that, in force of Eq. (7), $\gamma=\phi^e_x(0-)-\phi^e_x(0+)=\pm 4\ \mathrm{sech}\ \xi$; henceforth, the largest possible amplitude for the normalized bias $|\gamma_c|=4$ is achieved when $\xi=0$. For $\xi<0$ the phase in the origin grows above the threshold value $|\phi^e(0)|=\pi$ and the static solution in Eq. (10) is no longer stable: the two semifluxons develop into integer fluxons driven away in opposite directions under the effect of the Lorentz force associated with the bias current. According to Ref. 15 and from numerical simulations (reported later), we found that the instability arises when the amplitude of γ exceeds the critical value $\gamma_c=4$, corresponding to $I_c=\pm 4J_c\lambda_j W$. With such a notation $\gamma=\pm\gamma_c\ \mathrm{sech}\ \xi$, i.e., $\xi=\cosh^{-1}(\gamma_c/|\gamma|)$. The last expression allows us to find the dependence of $\phi^e(0)$ on γ; it is found that $\cos\phi^e(0)=1-2(\gamma/\gamma_c)^2$ [i.e., $\sin\phi^e(0)/2=\gamma/\gamma_c$]. Inserting the value $\gamma_c=4$ in Eq. (6), we find that for very long junctions the normalized zero-field critical current is inversely proportional to the junction length,

$$i_c(h=0)=\frac{\gamma_c}{l}, \tag{11}$$

as for an asymmetric inline junction[9] with the only difference that $\gamma_c=2$ in that case. Indeed, a long δ-biased JTJ in zero external field is equivalent to two inline asymmetric junctions in a parallel configuration; this is no longer true in presence of an external field h. For a generic γ value in the interval $[-4,4]$ the phase difference $\Delta\phi=\phi(0)-\phi(-\infty)=\phi(0)=2\ \sin^{-1}\gamma/\gamma_c$ corresponds to what in nowadays language is called a k-fractional vortex, where $k=\Delta\phi/(2\pi)=\pi^{-1}\sin^{-1}\gamma/\gamma_c$. Semi ($\xi=0$) and fractional ($\xi>0$) vortices are presently receiving a great deal of attention in the context of $0-\pi$ transition Josephson junctions.[12,25–27]

In summary, the main difference between short and long δ-biased JTJs is that in the former case the solution becomes unstable when $\gamma>\gamma_c=l$ and $\phi^e(0)>\pi/2$ while in the latter case the instability develops for $\gamma>\gamma_c=4$ and $\phi^e(0)>\pi$. The gradual crossover from intermediate to long JTJs has to be calculated numerically; it was found to be nicely described by the following empirically found relationships,

$$\gamma_c(h=0,l)=4\ \tanh\frac{l}{4}, \tag{12}$$

$$\phi^e_c(x=0,\ \ h=0,l)=\frac{\pi}{2}+\tan^{-1}\exp(l-\pi). \tag{13}$$

B. $h\neq 0$ and $\gamma=0$, $l/2>2\pi$

With $\gamma=0$, the Eq. (1) reduces to

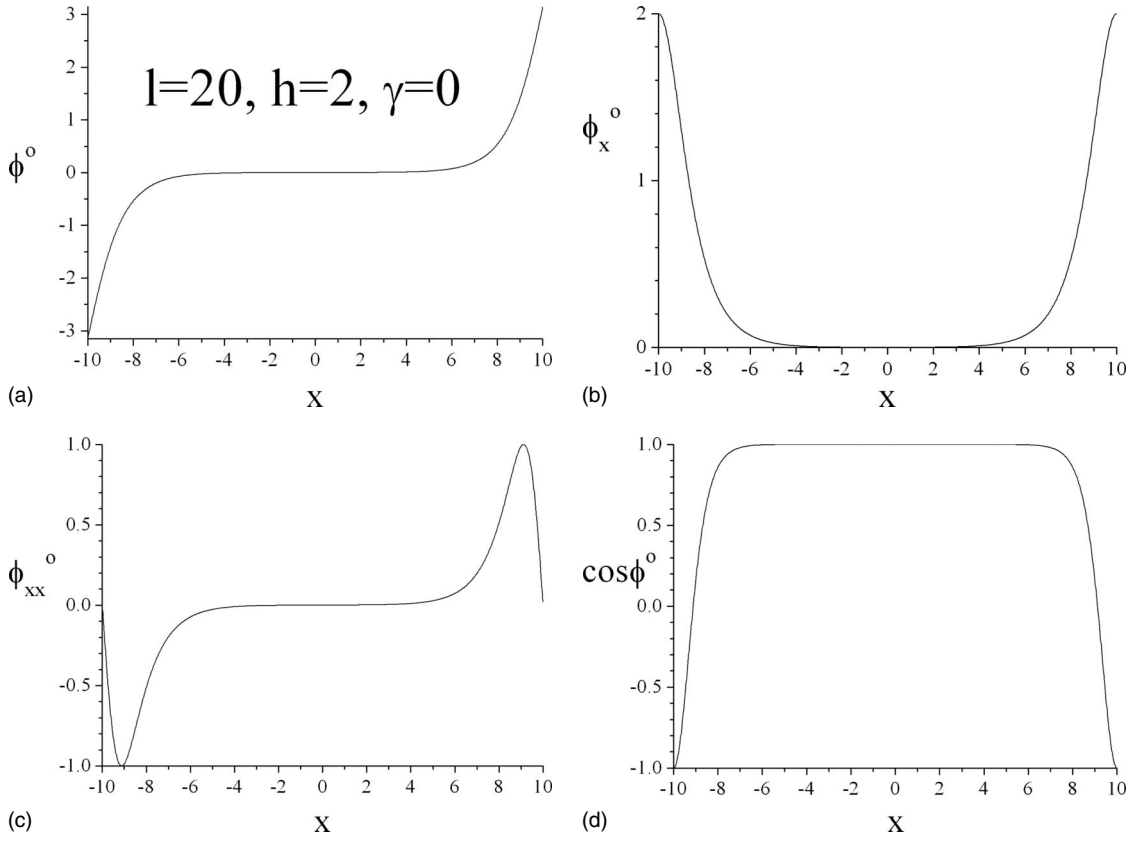

FIG. 4. (a) Phase profile $\phi^o(x)$ as in Eq. (15) for $\gamma=0$, $h=2$, and $l=20$, (b) its first derivative, (c) its second derivative, and (d) its cosines. Note that $\sin \phi^o(x)=\phi^o_{xx}(x)$ and $\cos \phi^o(x)=1-[\phi^o_x(x)]^2/2$.

$$\frac{d^2\phi}{dx^2} = \sin \phi(x). \tag{14}$$

Equation (14) was first introduced in the analysis of long asymmetric inline JTJs by Ferrel and Prange[9] in 1963; however, 4 years later Owen and Scalapino[14] reported an extensive study of its solutions for long symmetric inline JTJs: this is why Eq. (14) is commonly known as the Owen-Scalapino (OS) equation. With boundary conditions as in Eq. (5), the solution of the OS equation has to be an odd function $\phi^o(x)$ [i.e., with $\phi^o_x(x)$ even]. For given $h<2$ and $l>\pi/2$, exact solutions exists in terms of Jacobian elliptic functions. However, upon the assumption that the JTJ is so long that the magnetic field in its center can be neglected, $\phi^o_x(0)=0$, a simple approximate solution exists,

$$\phi^o(x) = \pm 4\left[\tan^{-1}\exp\left(x+\zeta+\frac{l}{2}\right) - \tan^{-1}\exp\left(-x+\zeta+\frac{l}{2}\right)\right], \tag{15}$$

in which the non-negative constant ζ is set by $h=\phi^o_x(\pm l/2) \approx \pm 2 \operatorname{sech} \zeta$ indicating that the largest possible amplitude of the normalized magnetic field is $h_c=2$ corresponding to $H_c=2J_c\lambda_j$ and $\zeta=0$. Now $\phi^o(0)=\pm 4[\tan^{-1}\exp(\zeta+l/2) - \tan^{-1}\exp(\zeta+l/2)]=0$. The sign in front of Eq. (15) now concords with that of the applied field. Equation (15) is shown in Fig. 4 for $l=20$ and $h=h_c$. Again Eq. (15), as Eq. (10), represents a superposition of two static fractional vortices, but now they a pinned at the junctions extremities and not in its middle point. As $|h|$ exceeds h_c, i.e., $\zeta<0$, we exit the Meissner regime and some magnetic flux enters into the junction interior; one (or more) integer vortices (fluxons) gradually develops at each extremity and move toward the center resulting in a phase profile that can no more be written in terms of Jacobian elliptic function. For $h \gg h_c$ the phase profile resulting from the superposition of several closely packed fluxons will be approximately linear $\phi^o(x)=hx$ and we recover the behavior of small JTJs (Fraunhofer regime).

The gradual crossover from intermediate to long JTJs has to be calculated numerically; here we anticipate that it was found to be nicely described by the following empirical relationship,

$$h_c(l) = \frac{2\pi}{l} + 2\tanh\frac{l}{2\pi},$$

in which the first (Fraunhofer) term dominates for small values of l, while the second (saturating) term dominates for large l values. It is worth to remark that if no current feeds a junction, then its electrode configuration does not affect the phase profile; in other words, inline, overlap and δ-biased JTJs all have the same phase profile as in Eq. (15) in presence of a given external magnetic field h; consequently, they also have the same (first) critical field.[15,22]

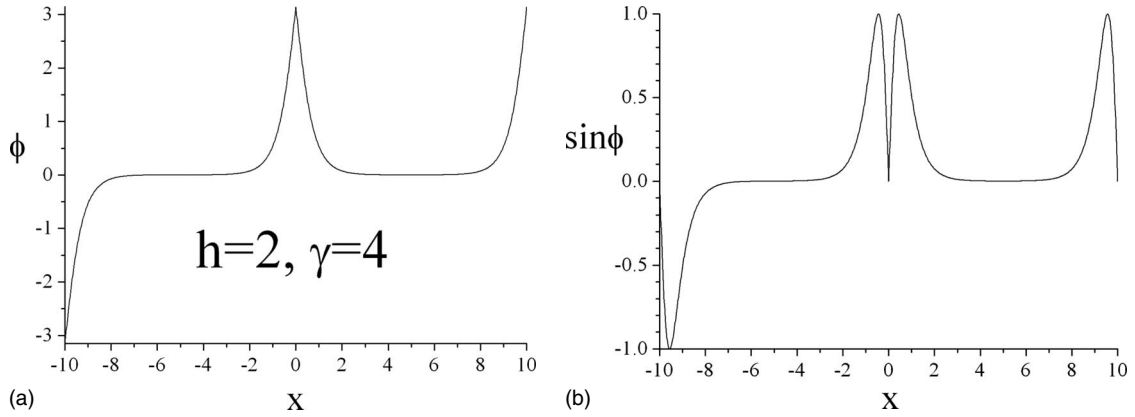

FIG. 5. (a) $\phi(x)$ as in Eq. (18) for $h=\gamma/2=2$ ($\zeta=\xi=0$) and $l=20$; (b) sin $\phi(x)$. Only the junction right side contributes to the Josephson current. It is sin $\phi(x)=\phi_{xx}(x)$ and cos $\phi=1-[\phi(x)]^2/2$.

C. $h\neq 0$, $\gamma\neq 0$, $l/4>2\pi$

Approximate static phase profiles for nonzero h and γ values are obtained observing that Eq. (1) can be rewritten as two identical, although independent, OS equations for the left ($-l/2\leq x<0$) and right ($0<x\leq l/2$) inline asymmetric half junctions each with an effective bias current $\gamma/2$. The boundary conditions for the left and right half junctions are simply given by Eqs. (5) and (9),

$$\left.\frac{d\phi}{dx}\right|_{x=-l/2}=h \quad \left.\frac{d\phi}{dx}\right|_{x=0}=\frac{\gamma}{2}, \tag{16}$$

$$\left.\frac{d\phi}{dx}\right|_{x=0}=-\frac{\gamma}{2} \quad \left.\frac{d\phi}{dx}\right|_{x=l/2}=h. \tag{17}$$

It is convenient to rewrite the constant C in Eq. (2) as $C=(2-k^2)/k^2$; for $C>1$, then $k^2<1$ and vice versa. According to the notation of Ref. 14, the above conditions can be rewritten in terms of Jacobian elliptic functions $\mathrm{dn}(x,k_d^2)$ and $\mathrm{cn}(x,1/k_c^2)$ of argument x and modulus k_d^2 and $1/k_c^2$, respectively. For $k_d\leq 1$,

$$\mathrm{dn}\left(\frac{l/2-x_{0d}}{k_d},k_d^2\right)=\frac{k_d}{2}h \quad \text{and} \quad \mathrm{dn}\left(\frac{-x_{0d}}{k_d},k_d^2\right)=\pm\frac{k_d}{2}\frac{\gamma}{2},$$

while for $k_c\geq 1$,

$$\mathrm{cn}(l/2-x_{0c},1/k_c^2)=\frac{k_c}{2}h \quad \text{and} \quad \mathrm{cn}(-x_{0c},1/k_c^2)=\pm\frac{k_c}{2}\frac{\gamma}{2}.$$

Being the above-mentioned elliptic functions limited to the $[-1,1]$ range, the solutions of the OS problem can be found as far as both $|h|$ and $|\gamma/2|$ are smaller than 2. Once $h\in[-2,2]$, $\gamma\in[-4,4]$ and $l>\pi$ are given, the couples (x_{0d},k_d) or (x_{0c},k_c) can be numerically found. This mathematical procedure allows to find many (sometime physically noninteresting) solutions and it is well known that the number of possible solutions increases with the junction normalized length.[28] For $l/2\gg 4\pi$, the approximate solution of Eq. (14) is

$$\begin{aligned}\phi(x)=&\pm 4\left[\tan^{-1}\exp(x-\xi)\right.\\&\left.-\tan^{-1}\exp\left(-x+\zeta-\frac{l}{2}\right)\right] \quad \text{for} \quad -l/2\leq x<0\\=&\pm 4\left[\tan^{-1}\exp(-x-\xi)\right.\\&\left.+\tan^{-1}\exp\left(x-\zeta-\frac{l}{2}\right)\right] \quad \text{for} \quad 0<x\leq l/2\end{aligned} \tag{18}$$

in which ξ and ζ are two non-negative independent constants; in fact, $\gamma\approx\pm 4$ sech ξ and $h\approx\pm 2$ sech ζ. If $h=0$, then $\zeta\to\infty$ and $\phi(x)=\phi^e(x)$. Vice versa, if $\gamma=0$, then $\xi\to\infty$ and $\phi(x)=\phi^o(x)$. In other words, the generic static phase profile of a long δ-biased junction in the Meissner state is obtained simply by the sum of (four) noninteracting fractional vortices. The sign in front of Eq. (18) concords with that of the product $h\gamma$. Looking at the Eqs. (16) and (17), it is seen that an interesting situation occurs when $h=\pm\gamma/2$. For $h=0$ the bias current γ flows symmetrically in the left and right junction sides [see Fig. 3(d)]. With $h\neq 0$ the symmetry is broken and the current flows mainly in one of the junction sides. When $|h|=\gamma/2\leq 2$, then $\zeta=\xi$ and the applied current only flows in one junction side, while in the other side the average Josephson current vanishes. For $h=\gamma/2=2$ ($\zeta=\xi=0$) the above expression for $\phi(x)$ and its sine are depicted in Figs. 5(a) and 5(b), respectively. Only the junction right side contributes to the Josephson current.

Let us remark that, being $|\gamma|\leq\gamma_c$, in force of Eq. (6), for the largest Josephson current i_c we have

$$|i_c(h)|=\frac{\gamma_c}{l}. \tag{19}$$

In other words, for long δ-biased JTJs in the Meissner state ($-2\leq h\leq 2$) the critical current is independent on the externally applied field. There is no other junction configuration for which this peculiarity occurs. The above result is only apparently in contrast with Kuprianov[14] quadratic prediction for infinitely long point-injected junctions

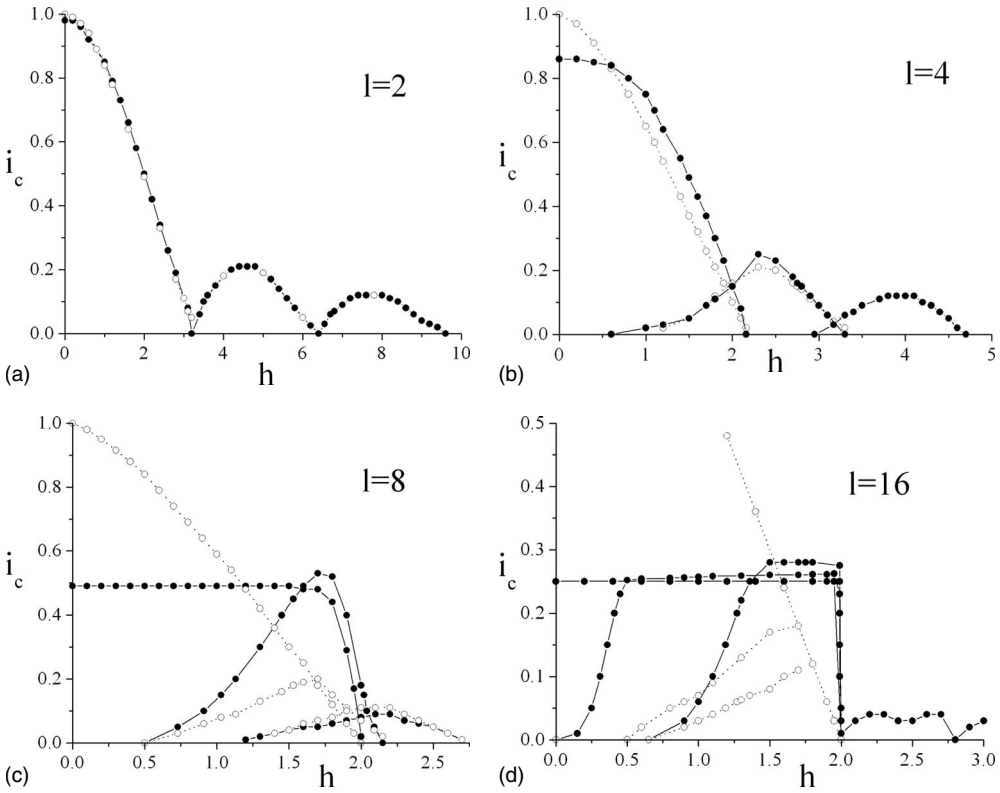

FIG. 6. Numerically computed magnetic diffraction patterns for different junction normalized lengths. From (a) to (d) i_c vs h, respectively, for $l=2,4,8,16$. The full dots refer to point-injected bias current, while, for the sake of comparison, the open dots correspond to the well-known case of a uniformly biased junction.

$$i_c(h) = \frac{2+\sqrt{4+h^2}}{l}, \tag{20}$$

leading to $i_c(\pm h_c)=(1+\sqrt{2})i_c(0)/2 \approx 1.2 i_c(0)$. In fact, Eq. (20) also takes in the account the penetration of fluxons into the barrier leading to the non-Meissner regime characterized by higher modes phase profiles[14] that will be discussed in the next section. In 1985 Radparvar and Nordman[16] reported the experimental magnetic diffraction pattern of a very long ($L \simeq 100\lambda_j$) Nb-Pb laterally injected JTJ in reasonable agreement with Eq. (20) despite their electrode configuration only roughly realized the point-injected approximation.

IV. STATIC NUMERICAL SIMULATIONS

In this section we discuss the numerically obtained solutions of the PDE in Eq. (1) with boundary conditions as in Eq. (5). The direct numerical integration of Eq. (1) poses large problems of stability due to the fact that there are no losses in the system; to avoid this problems, we recurred to the integration of the time-dependent perturbed sine-Gordon equation

$$\phi_{xx} - \phi_{tt} - \sin\,\phi = \gamma\delta(x) + \alpha\phi_t - \beta\phi_{xxt}, \tag{21}$$

with $\alpha=3$ in order to have a fast decay of the temporal features of the solution toward a static solution (in real device $\alpha \leq 0.01$). The term containing the surface losses was simply dropped to save computer time, i.e., $\beta=0$. Equation (21) has been numerically integrated by using the commercial finite-element simulation package of COMSOL MULTIPHYSICS (www.comsol.com) for different values of the normalized length l which enters the PDE through the boundary conditions. The δ function has been approximated by the continuous function $f(x)=\rho\ \mathrm{sech}^2(2\rho x)$ with the parameter $\rho=O(10^2)$ [note that $f(0)=\rho$, $f(1/\rho)=\rho\ \mathrm{sech}^2\ 2 \approx 0.07\rho$, and $\int_{-\infty}^{\infty} f(x)dx=1$].

In order to trace the different lobes of i_c vs h, it is crucial to start the numerical integration with a proper initial phase profile. As far as $l<\pi$ the initial condition for the numerical integration of Eq. (1) was simply set to $\phi(x)=0$. In order to find the several possible initial conditions for $l>\pi$, the OS problem was solved for a given value of h and with γ set to zero. Once the initial phase derivative was known, also the initial phase profile could be easily derived.[14] Finally, during the numeric calculation, γ was changed until the numerical solution becomes unstable. We have numerically computed γ_c as the maximum allowed value of the bias current for each chosen value of the magnetic field h. Once γ_c was found, the corresponding critical current i_c could be calculated either numerically or, in an equivalent manner, resorting to Eq. (6). As expected, a general peculiarity of the numerically found phase profiles for long enough δ-biased junctions is that the phase values at the junction extremities ($x=\pm l/2$) do not depend on γ; vice versa, the phase behavior near the origin does not depend on the applied field h.

Figures 6(a)–6(d) display the magnetic diffraction patterns for point-injected JTJs with different normalized lengths l. We remark that the $i_c(h)$ patterns are symmetric

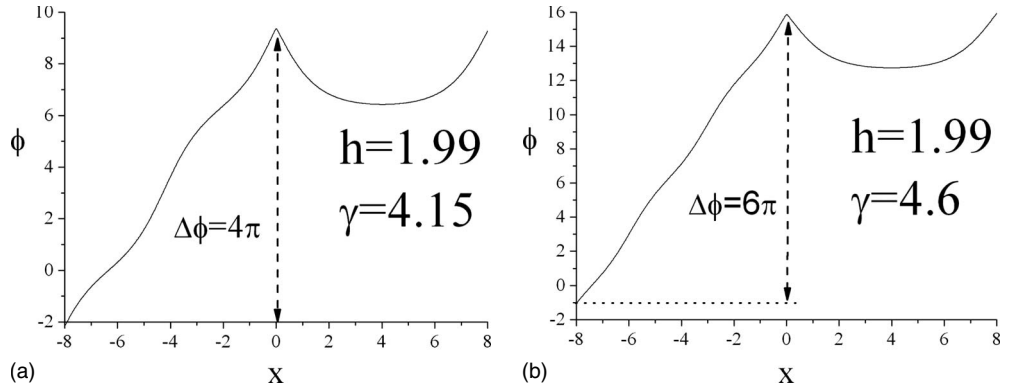

FIG. 7. Numerically computed phase profiles for higher-order modes with $l=16$ and $h=1.99$ and different γ values: (a) 2 vortex mode for $\gamma=4.15$ and (b) 3 vortex mode for $\gamma=4.6$.

around $h=0$. For comparison we also report the $i_c(h)$ for a uniform bias; more precisely, the full dots refer to the point-injected current, while the open (gray) dots correspond to the uniform bias. For $l=1$, the numerical data (not reported) closely follow the expected Fraunhofer-type dependence (with $h_c=2\pi$) with differences only in the third significant digit. As shown in Fig. 6(a), for $l=2$ we still have a Fraunhofer-type pattern. Pronounced deviations from the small junction behavior were found for $l=4$, but, as can be seen in Fig. 6(b), they disappear for large filled values. Increasing l, some ranges of magnetic field develop in correspondence of the pattern minima in which i_c may assume two (or more) different values corresponding to different phase profiles inside the barrier. In fact, each pattern lobe is associated with a given vortex structure; more precisely, in the first lobe which, for $l=4$, goes from $h=0$ to $h_c\approx 2.2$, the external magnetic field is shielded and vortex cannot penetrate into the barrier (Meissner state). However, at the very end of this lobe a fluxon is present in the junction. In the successive lobes the magnetic field penetrates into the barrier and vortices are created in the barrier in a way which closely recalls the behavior of the type-II superconductors, even though the vortices we are dealing with are quite different from the Abrikosov ones as they do not have a normal core. In the second lobe, moving from $h\approx 3$ to $h\approx 4.6$, we start from a phase configuration very similar to that at the right side of the first lobe in which one vortex is present in the barrier and we end up with two bunched fluxons. Adopting the terminology used in Ref. 14, we refer to the first (Meissner) lobe as to "0 to 1 vortex mode" lobe, the second as the "1 to 2 vortex mode" lobe, and so on. In general, one may talk about the "n to $n+1$ vortex mode" when the junction contains more than n but less than $n+1$ vortices. As l is increased from 4 to 8 drastic changes occur (the crossover point being approximately 2π), as shown in Fig. 6(c): the critical current get smaller and smaller, according to Eq. (11), and the principal lobe gets flatter and flatter resulting in a rather large plateau; further, the lobes broaden and overlap each other with h_c converging to 2. This behavior is even more pronounced for $l=16$ as shown in Fig. 6(d). In other words, the main (Meissner) lobe is a rectangle with corners in $h=0$ and 2 and $\gamma=0$ and 4. The phase profiles in the nontrivial corners are those already shown in Figs. 3–5.

The phase profile corresponding to the 2 and 3 fluxon modes are reported in Figs. 7(a) and 7(b), respectively, for $h(\gamma)$ slightly below (above) its critical value. It is evident that the vortices only penetrate in left side of the junction. However, the situation reverses by reversing either h or γ. The maximum supercurrent associated to a given vortex mode increases with the mode order; this is peculiar of δ-biased JTJs.

V. EXPERIMENTS

To investigate the properties of δ-biased JTJs, we have used are high-quality Nb/Al-Al_{ox}/Nb JTJs fabricated on silicon substrates using the trilayer technique in which the junction is realized in the window opened in a SiO insulator layer. We measured a large number of both linear and gapped annular junctions all of them with width $W=2$ μm but whose lengths varied from $L=80$ to 335 μm. The width of the electrodes carrying the current in and out of the barrier was 10 μm. The thickness of the SiO_2 insulator layer was 200 nm and the so-called "idle region," i.e., the overlapping of the wiring layer onto the base electrode was about 1 μm for all the junctions. In order to vary the sample normalized lengths over a large range values, we used two sets of samples having quite different critical current densities ($J_c=100$ A/cm^2 and 3 kA/cm^2), corresponding to $\lambda_j\simeq 80$ and $\simeq 12$ μm. In such a way samples were available with l spanning from about 1 to about 30. The values of the Josephson penetration depth λ_j were calculated taking into account the effect of the lateral idle region.[7,8] In Fig. 8 we report the log-log plot of the measured zero-field critical currents $i_c(0)$ of many δ-biased JTJs versus their reduced length L/λ_j. The critical current has been normalized to the small junction theoretical value calculated as the 70% of the current jump at the junction gap voltage. We observe that, for large normalized length, the experimental data clearly follow an inverse proportionality law as expected from Eq. (11) and the transition from long to short junctions is nicely fitted by the empirical expression in Eq. (12) (solid line).

On real samples, the measurements of maximum supercurrent against the external field often yield the envelop of the lobes, i.e., the current distribution switches automatically to the mode which for a given field carries the largest super-

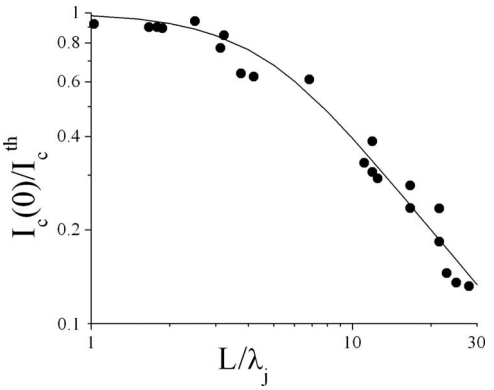

FIG. 8. Log-log plot of the measured zero-field critical currents $i_c(0)$ of many δ-biased JTJs versus their reduced length L/λ_j. The critical current has been normalized to the small junction theoretical value calculated as the 70% of the current jump at the junction gap voltage. The solid line is obtained from Eq. (11) with γ_c as in the empirical Eq. (12).

current. Sometimes, for a given applied field, multiple solutions are observed on a statistical basis by sweeping many times on the junction current-voltage characteristic. Figures 9(a)–9(d) display the measured magnetic diffraction patterns for four linear samples in a uniform in-plane field with selected normalized lengths. We found an excellent agreement with the results of numerical calculation discussed in the previous section. Marked deviation from the small junction Fraunhofer-type behavior were observed for $L=3\lambda_j$. It is evident that, for longer JTJs, the $I_c(H)$ is made of few flat segments corresponding to different static phase solutions containing more and more fluxons. Since the number of possible static solutions increases with the junction normalized length, it is straightforward to assume that, as l increases, the number of flat segments increases too, while their lengths decrease so that to merge in a monotonically increasing critical current as predicted in Ref. 14 and observed in Ref. 16. We also note some similarity with the flux-flow oscillator pattern reported in Fig. 18 of Ref. 29.

As shown in Fig. 10, analogous results were obtained for samples with the gapped annular geometry in a radially uniform, although uncalibrated, magnetic field. As explained in Sec. I the radial field was obtained by applying a uniform magnetic field perpendicular to the superconducting ring which constitutes the base electrode of the junction itself. The asymmetry of both diffraction patterns is an extrinsic self-field effect due to the configuration of the current-carrying leads on the chip.

The dynamic of a δ-biased JTJ was also investigated both experimentally and by numerically integrating the time-dependent Eq. (21) whose steady-state solutions were typical of a soliton moving in a two-level potential with the flux-on(s) being accelerated only when passing trough the origin. We have focused out attention on the zero-field single fluxon shuttling mode. Figure 11 compares the first zero-field step

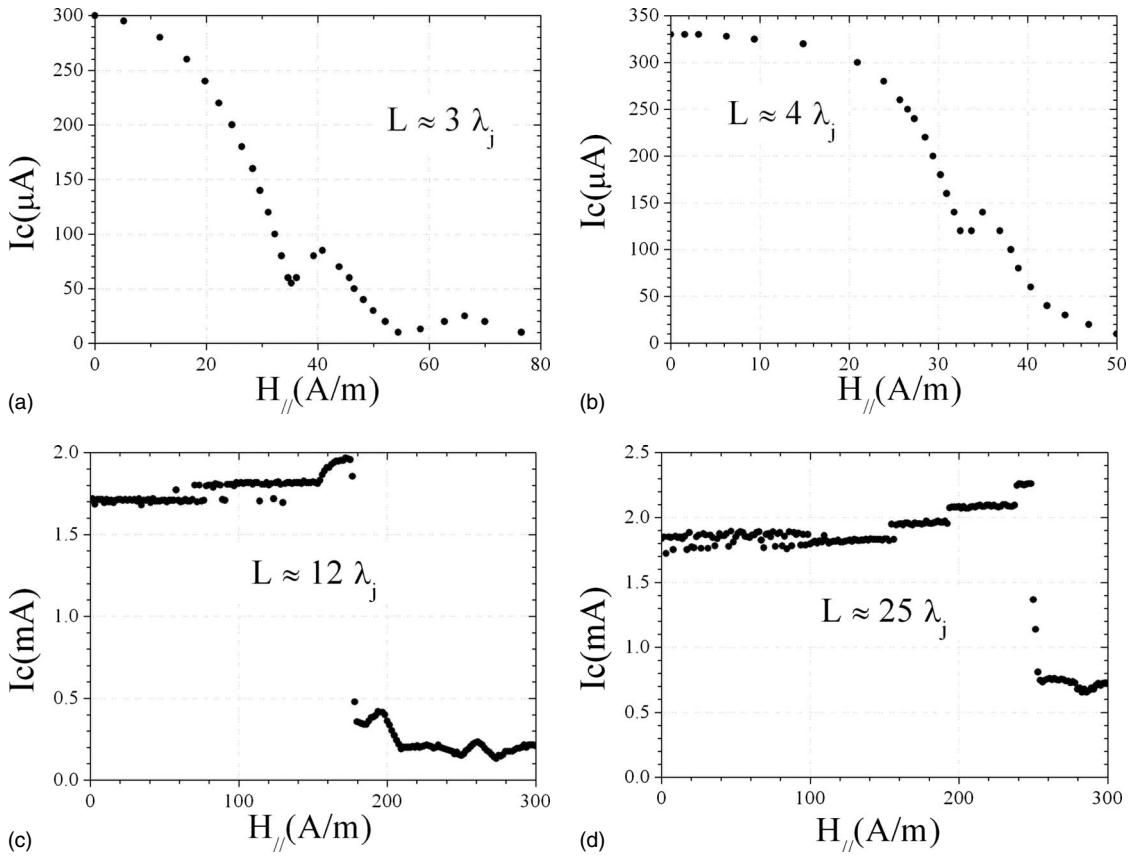

FIG. 9. Experimental magnetic diffraction patterns taken for linear samples in a uniform in-plane field with increasing normalized lengths $l=L/\lambda_j$. (a) $L=250$ μm and $\lambda_j \simeq 80$ μm, (b) $L=300$ μm and $\lambda_j \simeq 80$ μm, (c) $L=150$ μm and $\lambda_j \simeq 12$ μm, and (d) $L=300$ μm and $\lambda_j \simeq 12$ μm.

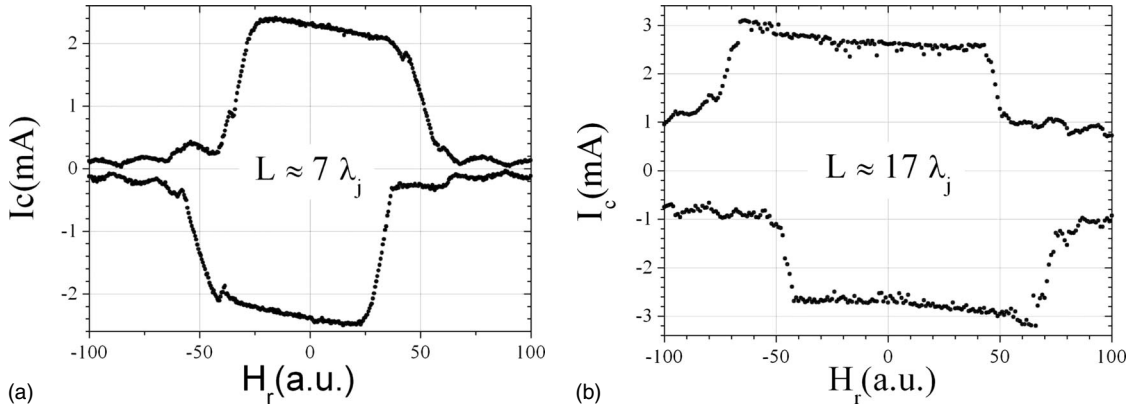

FIG. 10. Experimental magnetic diffraction patterns in a radially uniform magnetic field H_r for two gapped annular samples having the same critical current density $J_c=3$ kA/cm^2 (corresponding to $\lambda_j \simeq 12$ μm) and different lengths L. (a) $L=82$ μm and (b) $L=200$ μm.

profiles of a δ-biased (solid line) and a uniformly biased (dashed line) long overlap JTJs having the same length ($L=150$ μm) and the same Josephson current density ($J_c=3$ kA/cm^2). The data were taken a $T \approx 6$ K. Contrary to the case of uniform bias, a current threshold value is needed to avoid that fluxon stops due to friction. This value, of course, depends on the junction length and losses: the longer the junction, the smaller should the losses be to maintain a finite-voltage dynamic steady state. The $\gamma - \langle \phi_t \rangle$ plot, corresponding to the zero-field step profile, is smoother than that obtained when the bias is uniform and is characterized by fine structures associated to the fluxon interactions with plasma waves[30,31] originated by the fluxon itself when passing across the potential discontinuity. Often the back-switching transition has been observed at the top of the step, as indicated by the solid arrow pointing to the zero voltage state. As a matter of fact, point-injected junctions seem not to reveal new dynamical states. We only remark that *displaced linear slopes*[22] were numerically found and experimentally regularly observed in absence of magnetic field and for junction with large losses ($\alpha \approx 1$ or $T > 0.7T_c$). when the dc bias exceeded its critical value. Displaced linear slopes were also observed in the presence of a magnetic field which, by increasing the field further, eventually develops in large amplitude flux flow steps.

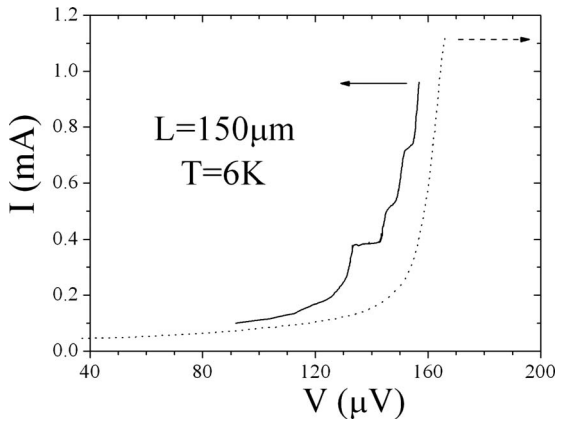

FIG. 11. Profiles of the first zero-field step for overlap junctions with $L=150$ μm and $J_c=3$ kA/cm^2 (corresponding to $\lambda_j \simeq 12$ μm). (a) δ bias (solid line) and (b) uniform bias (dashed line). The data were taken a $T \approx 6$ K. The arrows indicate the switching direction at the top of the step.

VI. CONCLUSIONS

In this paper we focused on δ-biased (or point-injected) long Josephson tunnel junctions. Our analysis goes much beyond the previous theoretical[14] and experimental[16] works in which only extremely long junctions were treated. We considered a linear JTJ in a uniform magnetic field and a gapped annular junction in a radially uniform field. These two electrode configurations [shown in Figs. 1(a) and 1(b), respectively] are topologically equivalent, that is, they are described by the same partial differential equation [Eq. (1)] with the same boundary conditions [Eq. (5)]. Apart from their intriguing physical properties, the interest for δ-biased JTJs stems from the fact that they were successfully used to detect trapped fluxoids in a recent experiment aimed to study the spontaneous defect production during the fast quenching of a superconducting loop.[1] The main peculiarity of a δ-biased junction is the jump of the phase derivative at the point were the current is injected. We have shown that this discontinuity naturally leads to the formation of fractional vortices. In the last few years there has been a great deal of interest in the phase discontinuity observed in $0-\pi$ transition junctions which can be modeled with a bias made of two closely spaced δ functions with opposite sign, more precisely by the derivative of a δ function.[32] We believe that our findings on the properties of a *single* δ function can shed some more light on the mechanisms responsible of the appearance of fractional vortices in $0-\pi$ transition Josephson tunnel junctions.

ACKNOWLEDGMENTS

The authors thank A. Gordeeva for useful discussions and for helping us with the dynamical numerical simulations. One of us (V.P.K.) acknowledges the financial support from the Russian Foundation for Basic Research under the Grants No. 09-02-00246 and No. 09-02-12172.

*roberto@sa.infn.it

[1] R. Monaco, J. Mygind, R. J. Rivers, and V. P. Koshelets, Phys. Rev. B **80**, 180501(R) (2009).
[2] J. R. Kirtley and F. Tafuri, Phys. **2**, 92 (2009).
[3] W. H. Zurek, Phys. Rep. **276**, 177 (1996).
[4] T. W. B. Kibble, Phys. Rep. **67**, 183 (1980).
[5] N. Martucciello and R. Monaco, Phys. Rev. B **54**, 9050 (1996).
[6] G. S. Lee and A. T. Barfknecht, IEEE Trans. Appl. Supercond. **2**, 67 (1992).
[7] R. Monaco, G. Costabile, and N. Martucciello, J. Appl. Phys. **77**, 2073 (1995).
[8] A. Franz, A. Wallraff, and A. V. Ustinov, J. Appl. Phys. **89**, 471 (2001).
[9] R. A. Ferrel and R. E. Prange, Phys. Rev. Lett. **10**, 479 (1963).
[10] D. L. Stuehm and C. W. Wilmsem, J. Appl. Phys. **45**, 429 (1974).
[11] C. S. Owen and D. J. Scalapino, Phys. Rev. **164**, 538 (1967).
[12] E. Goldobin, N. Stefanakis, D. Koelle, and R. Kleiner, Phys. Rev. B **70**, 094520 (2004).
[13] E. Goldobin, H. Susanto, D. Koelle, R. Kleiner, and S. A. van Gils, Phys. Rev. B **71**, 104518 (2005).
[14] M. Yu. Kuprianov, K. K. Likharev, and V. K. Semenov, Fiz. Nizk. Temp. **2**, 1252 (1967) [Sov. J. Low Temp. Phys. **2**, 610 (1976)].
[15] K. K. Likharev, *Dynamics of Josephson Junctions and Circuits* (Gordon & Breach Science, New York, 1984).
[16] M. Radparvar and J. E. Nordman, IEEE Trans. Magn. **MAG-21**, 888 (1985).
[17] B. D. Josephson, Rev. Mod. Phys. **36**, 216 (1964).
[18] M. Weihnacht, Phys. Status Solidi **32**, K169 (1969).
[19] Nadia Martucciello and Roberto Monaco, Proceedings of the 21st International Conference on Low Temperature Physics, Prague, 1996 [Czech. J. Phys., Sect A 46, 651 (1996)].
[20] E. H. Brandt and J. R. Clem, Phys. Rev. B **69**, 184509 (2004), and references therein.
[21] A. Barone, W. J. Johnson, and R. Vaglio, J. Appl. Phys. **46**, 3628 (1975).
[22] A. Barone and G. Paternò, *Physics and Applications of the Josephson Effect* (Wiley, New York, 1982).
[23] H. Tamura and Y. Matsuda, Bull. JSME **30**, 482 (1987).
[24] D. W. Jordan and P. Smith, *Nonlinear Ordinary Differential Equations* (Claredon, Oxford, 1987).
[25] N. Lazarides, Phys. Rev. B **69**, 212501 (2004).
[26] J. R. Kirtley, K. A. Moler, and D. J. Scalapino, Phys. Rev. B **56**, 886 (1997).
[27] E. Goldobin, D. Koelle, and R. Kleiner, Phys. Rev. B **66**, 100508(R) (2002).
[28] Let us remind that for $k_c<1$, $\mathrm{cn}(u,1/k_c^2)$ is a periodic odd function with period $U_c=4K(1/k_c^2)$ and, for $k_d<1$, $\mathrm{dn}(u,k_d^2)$ is periodic even with period $U_d=2K(k_d^2)$ (where $K(k^2)$ is the complete elliptic integral of first kind: $k^2\in[0,1]$ and $K(k^2)\in[\pi/2,\infty]$). In the limit $k_{c,d}\to 1$ (corresponding to the limit $l\to\infty$), the period diverges and $\mathrm{cn}(u,1)=\mathrm{dn}(u,1)=\mathrm{sech}\,u$.
[29] Valery P. Koshelets and Jesper Mygind, in *Studies of High Temperature Superconductors*, edited by A. V. Narlikar (NOVA Science, New York, 2001), Vol. 39, pp. 213–244.
[30] A. A. Golubov and A. V. Ustinov, IEEE Trans. Magn. **MAG-23**, 781 (1987); A. A. Golubov, I. L. Serpuchenko, and A. V. Ustinov, Zh. Eksp. Teor. Fiz. **94**, 297 (1988) [Sov. Phys. JETP **67**, 1256 (1988)].
[31] P. Barbara, R. Monaco, and A. V. Ustinov, J. Appl. Phys. **79**, 327 (1996); R. Monaco, P. Barbara, and J. Mygind, Phys. Rev. B **47**, 12292 (1993).
[32] K. Vogel, W. P. Schleich, T. Kato, D. Koelle, R. Kleiner, and E. Goldobin, Phys. Rev. B **80**, 134515 (2009), and references therein.